Anal. Chem. **2001,** *73,* 1240−1246

Generation of Gradients Having Complex Shapes Using Microfluidic Networks

Stephan K. W. Dertinger, Daniel T. Chiu, Noo Li Jeon, and George M. Whitesides*

Department of Chemistry and Chemical Biology, Harvard University, 12 Oxford Street, Cambridge, Massachusetts 02138

This paper describes the generation of gradients having complex shapes in solution using microfluidic networks. Flowing multiple streams of fluid each carrying different concentrations of substances laminarly and side-by-side generated step concentration gradients perpendicular to the direction of the flow. Appropriately designed networks of microchannels for controlled diffusive mixing of substances generated a range of shapes for the gradients, including linear, parabolic, and periodic. The lateral dimensions of the gradients ranged from 900 to 2200 μm. This paper also demonstrates the generation of overlapping gradients composed of different species. Since solutions in the microfluidic network exist as steady states and are continuously renewed, the gradients established in the capillaries are spatially and temporally constant and can be maintained easily for periods of hours. Using laminar flow to generate gradients should be useful in both biological and nonbiological research.

Gradients of diffusible substances having chemoattractant or chemorepellent properties play an important role in biological pattern formation[1] and morphogenesis;[2] angiogenesis[3] and axon pathfinding[4,5] provide examples of processes that require gradients. Despite the importance of gradients in biology, there are only a few techniques capable of generating and maintaining them easily in solution. Techniques using chemataxis chambers (i.e., the Boyden chamber[6] or modifications of it[7,8]) or using pipets to release diffusible substances[5] are limited in their capability to generate gradients of different shapes and in their ability to maintain gradients over long periods of time. Efforts to investigate the role of gradients in biology would benefit from a technique that could generate gradients with complex shapes for correlating the shape of biologically active gradients and the behavior of cells in them. The ability to superimpose multiple gradients of different substances would provide a way to quantify and compare the role of competing gradients; such complex heterogenities in concentrations are ubiquitous in higher organisms.[2]

The main challenge in generating gradients of complex shapes in solution is that gradients evolving from point sources and line sources develop bell-shaped concentration profiles.[9] The only practical way to overcome this restriction and to generate gradients with more shapes is to superimpose multiple bell-shaped gradients of different amplitude evolving from different positions. This type of process requires a high degree of control over the position of the individual sources, as well as the quantity of substances they release; conventional techniques lack the appropriate accuracy and stability.

To maintain the shape of a gradient over time, it is necessary to reach a steady state in which the quantity of substances released into and removed from the system is balanced. If the balance is imperfect, concentrations change over time. Most current techniques used for generating gradients in solution suffer from the inability to maintain their profiles over long periods of time.

Using a microfluidic approach we have decribed previously,[10] it is possible to generate spatially and temporally constant gradients extending over hundreds of micrometers and to maintain their shapes over long periods of time. The laminar flow of fluids in small capillaries permits multiple streams of solutions containing different concentrations to flow side by side without turbulence.[11,12] By controlling the chemical composition of the individual streams, a broad variety of concentration profiles can be created perpendicular to the direction of flow. The continuous movement of solution through the capillaries leads quickly to a steady state. Since only minute amounts (μL) of liquids are used in these microfluidic systems, this approach is applicable even for costly substances.

In this paper, we extend our previous work[10] and demonstrate the generation of gradients with complex shapes in solution using networks of microchannels designed to control diffusive mixing of substances. This paper describes these systems and includes a theoretical treatment with which to calculate the shapes of the gradients that they can generate. This treatment describes the blurring of the gradients due to diffusion in the channels. It also illustrates the overlay of multiple gradients. We believe the technique that forms the basis of these demonstrations provides

* To whom correspondence should be addressed: E-mail: gwhitesides@gmwgroup.harvard.edu. Fax: (617) 495−9857. Tel: (617) 495−9430.

(1) Meinhardt, H. *J. Cell Sci.* **1999**, *112*, 2867−2874.
(2) Neumann, C.; Cohen, S. *Bioessays* **1997**, *19*, 721−729.
(3) Carmeliet, P. *Nat. Med.* **2000**, *6*, 389−395.
(4) Baier, H.; Bonhoeffer, F. *Science* **1992**, *255*, 472−475.
(5) Song, H. J.; Poo, M.-M. *Curr. Opin. Neurobiol.* **1999**, *9*, 355−363.
(6) Boyden, S. *J. Exp. Med.* **1962**, *115*, 453−466.
(7) Zigmond, S. H. *J. Cell Biol.* **1977**, *75*, 606−616.
(8) Zicha, D.; Dunn, G. A.; Brown, A. F. *J. Cell Sci.* **1991**, *99*, 769−775.
(9) Crank, J. *The Mathematics of Diffusion*; Oxford University Press: Oxford, U.K., 1975.
(10) Jeon, N. L.; Dertinger, S. K. W.; Chiu, D. T.; Choi, I. S.; Stroock, A. D.; Whitesides, G. M. *Langmuir* **2000**, *16*, 8311−8316.
(11) Kenis, P., K. A.; Ismagilov, R. F.; Whitesides, G. M. *Science* **1999**, *285*, 83−85.
(12) Takayama, S.; McDonald, J. C.; Ostuni, E.; Liang, M. N.; Kenis, P. J.; Ismagilov, R. F.; Whitesides, G. M. *Proc. Natl. Acad. Sci. U.S.A.* **1999**, *96*, 5545−5548.

10.1021/ac001132d CCC: $20.00
Published on Web 02/16/2001

a new tool in investigating chemotaxis[13,14] and in other areas involving gradients (both biological and nonbiological), since it offers both a high degree of control over the shapes of gradients and high flexibility in their dynamic modification.[10]

MATERIALS AND METHODS

Fabrication of the Microfluidic Network. All microfluidic devices were fabricated in poly(dimethylsiloxane) (PDMS) using rapid prototyping[15−17] and soft lithography.[18] Briefly, a high-resolution printer was used to generate a mask (in the form of a transparency) from a CAD file. The transparency mask (which can have a minimum feature size of ∼20 μm, when generated by a 3300 dpi printer) was used in 1:1 contact photolithography with SU-8 photoresist (MicroChem, Newton, MA) to generate a negative "master", consisting of patterned photoresist on a Si wafer. Positive replicas with embossed channels were fabricated by molding PDMS against the master.[15−17] Inlet and outlets (1-mm-diameter holes) for the fluids were punched out of the PDMS using a sharpened needle. The surface of the PDMS replica and a clean glass substrate were activated in an air plasma (2 Torr, 60 s, 100 W) and brought together immediately after activation. An irreversible seal was formed between the PDMS and the glass substrate;[17] this assembly produced the required systems of microfluidic channels. Polyethylene tubing with outer diameter slightly larger than the inner diameter of the port was inserted into the hole to make the fluidic connections. The pieces of tubing were then connected to a syringe pump (Orion Sage, M362) to complete the fluidic device.

Analysis of the Data. We calibrated the relative fluorescence intensity in the channels after each experiment by flowing solutions of fluorescein of different concentrations in buffer through the network. Using this approach, we compensated for the inhomogeneous UV illumination of the microscope and the nonlinear response of the CCD camera to fluorescence intensities. Data analysis and mathematical calculations were done with IGOR PRO and LabVIEW.

RESULTS AND DISCUSSION

Network of Capillaries. Figure 1a shows a photograph of a representative microfluidic network used for generating gradients. This network generates a gradient in green and red dye. The three incoming channels at the top of the photograph contained green (left), a mixture of 1:1 green and red (middle), and red dye (right) into the network. We used a syringe pump to drive the fluid. As the streams of dye travel down the network, they are repeatedly split at the nodes, combined with neighboring streams, and allowed to mix by diffusion in the serpentine channels. In each layer, neighboring streams carrying different concentrations of diffusible substances are mixed in proportions equal to the splitting ratios at each node. At the end of the pyramidal network, all streams carrying different concentrations of green and red dye combined in a broad channel. The initial step profile of concentration at the inlets of the broad channel blurs due to diffusion as the stream flows down the channel. Since diffusion is slow relative to the time required to move through the channels, the concentration gradient perpendicular to the direction of flow is maintained in the broad channel. A small molecule (e.g., fluorescein) diffuses ∼55 μm within 1 s (using $D = 5.0 \times 10^{-6}$ cm^2/s for fluorescein[19]). The rate of flow we commonly used in our experiments was 1.2 mm/s. At the end of the broad channel, the fluid is collected in a waste reservoir. The concentration profile at a particular section across the small channels of the network or the broad channel is constant over time (that is, the concentrations within the channel are at steady state), because the solutions are continuously added and removed from the system.

The purpose of this microfluidic network (Figure 1a) is to split, combine, and mix the solutions introduced at the inlet in a controlled way. While keeping the number of inlets low, the splitting in the pyramidal network increases the number of streams carrying different concentrations and being brought together in the broad channel. As a result, complex gradients can be approximated with step-gradients made of a large number of small steps.

To calculate the concentration profiles at the outlets of the network, it is necessary to know the relative ratios at which the streams are mixed together in the long serpentine channels. The mixing ratios are governed by the splitting ratios of the streams at the branching points in the network. To derive the equation for the splitting ratios, we used the following definitions: We call a network having l input ports and m outputs that are combined in a broad channel a l-input/m-output network. Figure 1a shows a 3-input/9-output network. We define the part of the network that contains n vertical serpentine channels as a branched system of nth order ($B = n$). Within each branched system of nth order, we label the vertical serpentine channels (V) from the left to the right, starting with $V = 0$ and ending with $V = B - 1$. The branching points in a branched system are at the end of the serpentine channels. The nomenclature we introduced for the description of the network is summarized in Figure 1b. The design of the network we used throughout this work follows two general rules. First, the number of serpentine channels within a branched system increases by one going from a branched system of order n to a branched system of order $(n + 1)$. Second, in a network with n inlets, the first branched system is of order $(n + 1)$. For example, the first layer in a network having 3 inlets is of order 4 and consists of 4 serpentine channels. Third, all serpentine channels within a branched system have the same length and dimensions and thereby have the same resistivity for the fluids.

Since the fluidic resistivity of the horizontal channels connecting the serpentine channels (width, 100 μm; height, 45 μm; length, 375 μm) is negligible in comparison with the resistivity of the long, serpentine channels (width, 45 μm; height, 45 μm; length, ∼9.25 mm), an equivalent circuit (in analogy to the description of electrical networks) for the mathematical analysis can be approximated by taking into account the resistivity of the serpentine channels only. Furthermore, the resistivity of the serpentine channels is the same within each branched system (and over the entire network); this fact forces the incoming streams in one

(13) Arkowitz, R. A. *Trends Cell Biol.* **1999**, *9*, 20−27.
(14) Grebe, T. W.; Stock, J. *Curr. Biol.* **1998**, *8*, R154−R157.
(15) Qin, D.; Xia, Y.; Whitesides, G. M. *Adv. Mater.* **1996**, *8*, 917−921.
(16) Duffy, D. C.; McDonald, J. C.; Schueller, O. J. A.; Whitesides, G. M. *Anal. Chem.* **1998**, *70*, 4974−4984.
(17) McDonald, J., C.; Duffy, D. C.; Anderson, J. R.; Chiu, D. T.; Wu, H.; Schueller, O. J. A.; Whitesides, G. M. *Electrophoresis* **2000**, *21*, 27−40.
(18) Xia, Y.; Whitesides, G. M. *Angew. Chem., Int. Ed.* **1998**, *37*, 550−575.
(19) Cheng, Y. F.; Wu, S.; Chen, D. C.; Dovichi, N. J. *Anal. Chem.* **1990**, *62*, 496−503.

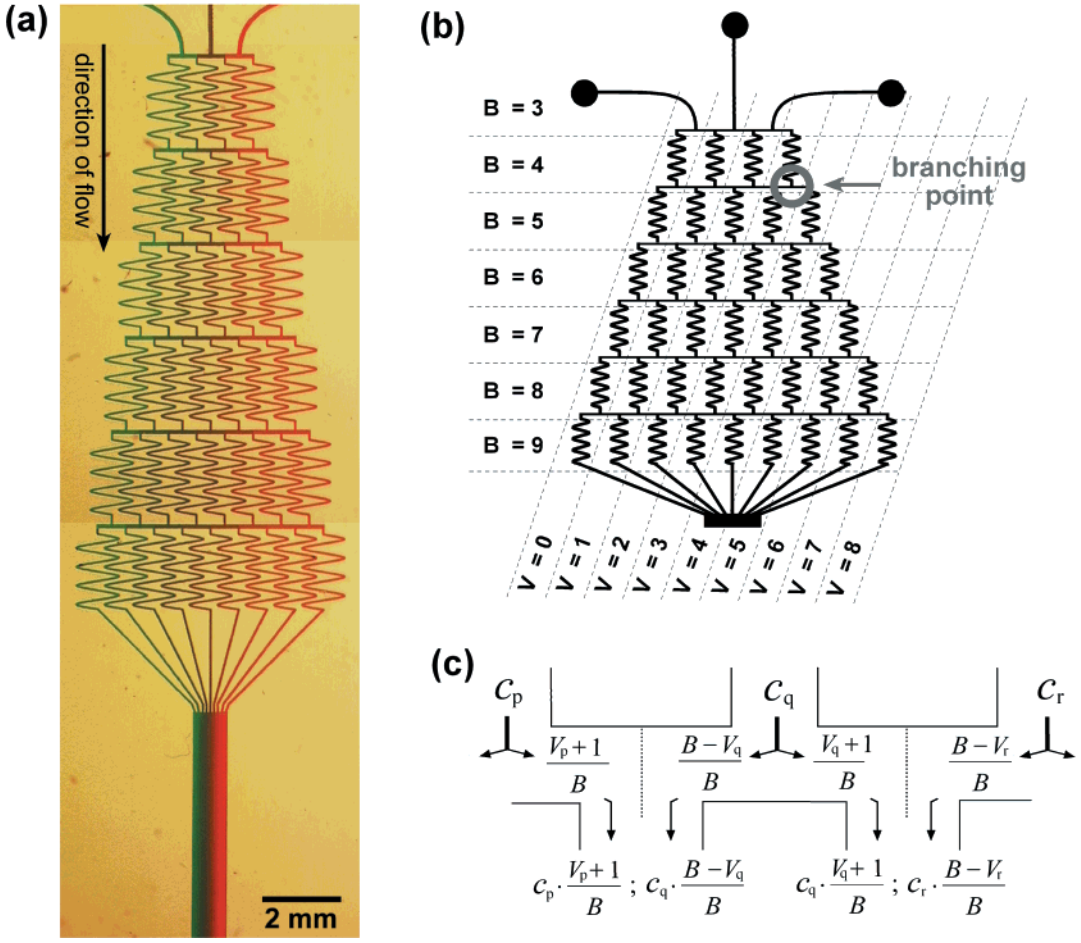

Figure 1. (a) Photograph showing a microfluidic device we used for generating gradients of green and red dyes in solution. The three incoming channels (top part of the photograph) were connected to syringes via tubings (not visible). After combining the streams into a single, wide channel (bottom of the photograph shown in (a)), a gradient was formed across the channel, perpendicular to the direction of flow. (b) Schematic explaining the nomenclature we used for the mathematical description of the network. (c) Schematic demonstrating the application of the formulas (eq 1 and eq 2) governing the splitting ratios at the branching points. The dotted lines indicate the boundary between the two combined streams. The concentrations at the end of the serpentine channels can be calculated by multiplying the concentration of the incoming streams (c_p, c_q, c_r) with the corresponding numbers of the splitting ratio (($V_p + 1$)/B, ($B - V_q$)/B, ($V_q + 1$)/B, and ($B - V_r$)/B, as indicated).

branched system to distribute equally among the serpentine channels of the following branched system. As a result, the flux of fluid through each serpentine channel of a branched system is equal. The vertical mirror symmetry of the network demands that the splitting ratios are symmetric with respect to the axis of symmetry. By combining all of these boundary conditions, we derived the following recursive formula governing the splitting ratios at the branching points. The portion of the stream that turns left is given by eq 1 and the portion that turns right by eq 2.

$$(B - V)/B \quad (1)$$

$$(V + 1)/B \quad (2)$$

Here B is the order of the branched system and V is the vertical channel within the branched system. The splitting ratios are normalized to $(B + 1)/B$ (i.e., $(B - V)/B + (V + 1)/B = (B + 1)/B$). We chose this normalization because it simplifies the calculations of the concentrations of the streams; the splitting ratio is also the factor by which the stream is diluted by the neighboring stream with which it has to share the serpentine channel of the following branched system (Figure 1c).

Throughout this work we used flow rates that guarantee a complete (99%) diffusive mixing of the fluids in the sepentine channels. A complete mathematical decription of diffusive mixing in the network, and a definition of percent mixing, are given elsewhere.[10]

The stepwise increase of the number of serpentine channels causes a corresponding decrease in flow rate when progressing from a branched system with n serpentine channels to the following branched system having $n + 1$ serpentine channels. The relative change of the flow rate is governed by the ratio $n/(n + 1)$. As long as complete diffusive mixing is ensured in all serpentine channels of the network, the flow rate in the network does not effect the concentration profile generated in the broad channel.

Shapes of Concentration Profiles. The shape of the concentration profile created at the junction of the broad channel is governed by the splitting ratios of the streams at the individual nodes in the pyramidal network and depends on the number of inlets of the network as well as on the relative concentrations of the solutions that are fed into the network. In general, the larger the number of inlets, the broader the range of accessible shapes.

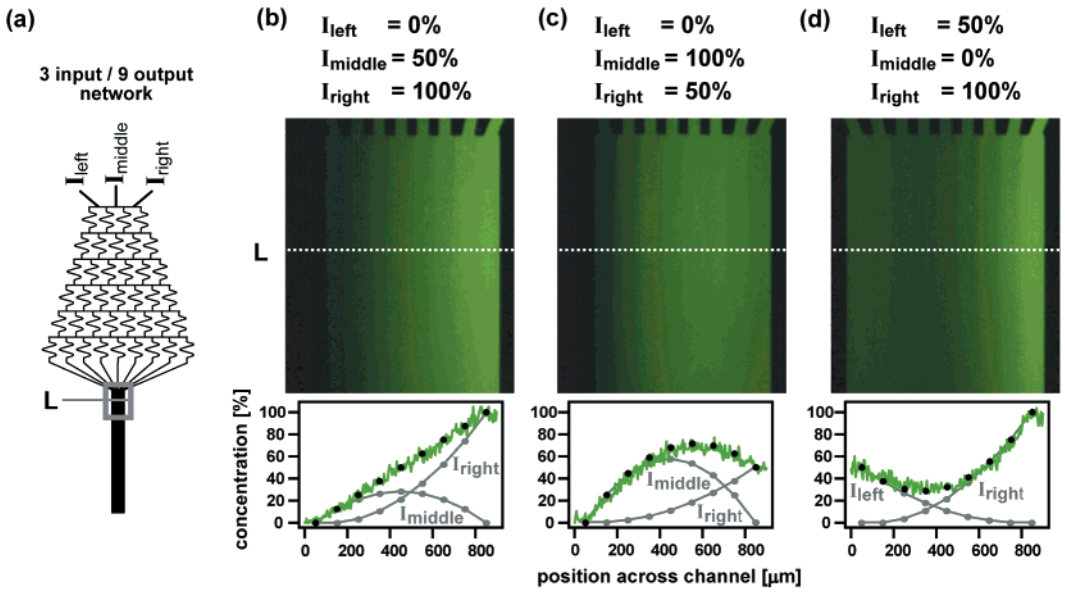

Figure 2. Fluorescence micrographs showing (b) linear and (c, d) parabolic gradients of fluorescein in solution. The microfluidic network we used for generating these gradients had 3 inlets and 9 outlets (a). The concentration of the solutions we introduced into each inlet of our microfluidic network is indicated above the micrographs. The plots below the micrographs show the corresponding fluorescence intensity profile (green line) across the broad channel (900 μm wide) 500 μm downstream (L, white dotted line) from the junction. The theoretically calculated concentration profiles of fluorescein are shown as black, round dots. The gray lines and dots in the graphs show the calculated contribution of the individual inputs to the overall profile. The flow rate in the broad channel is 1 mm/s.

The number of outputs determines the number of steps that compose a profile. The width of the broad channel defines the overall width of the profile. Changing the number of outputs does not effect the overall shape of the profile.

Due to the varying splitting ratios at the branching points in the network, streams injected from different inlets were mixed in different ways with neighboring streams while flowing through the network. As a result, depending on which inlet is the starting point for a solution, different concentration profiles are generated. In general, all accessible concentration profiles that can be generated using a *n*-input network can be expressed as a linear combination of the profiles generated by using the individual inputs.

By using the recursive formulas (eqs 1 and 2), we numerically simulated the accessible concentration profiles for a number of different networks and different concentrations at the inlets. We found empirically that all calculated concentration profiles generated by a microfluidic device having n inlets lie on a curve described by a polynomial of $(n - 1)$th order (a polynomial of nth order is defined by the following: $f(x) = a_0 + a_1x + a_2x^2 + ... + a_nx^n$).

Figure 2 shows the concentration profiles we generated using a network having three inlets and nine outlets; the gradients were obtained by permuting the order at the inlets of three different solutions containing 100, 50, and 0% fluorescein (fluorescein in 100 mM $NaHCO_3$ buffer, pH 8.3). Consistent with our empirical finding, all profiles of concentrations generated at the outlets of the network could be described by polynomials of second order. Figure 2b represents a special case, since a linear gradient can be completely described by a polynomial of first order (a polynomial of first order is a special case of polynomial of second order). In all cases, calculated concentrations (black, round dots in the graphs of Figure 2) and experimentally observed concentrations (green lines in the graphs of Figure 2) were in good agreement. The contributions of the individual inlets to the overall profile (black lines) are depicted in the bottom graphs of Figure 2 as gray lines and dots.

The fact that the mixing in our network leads to concentration profiles that can be described by polynomials rather than by binomial distributions (a binomial distribution is generated when the splitting ratios are 1:1 over the entire pyramidal network) is caused by the dependence of the splitting ratios at the nodes on their positions in the pyramidal network. The larger the distance of the nodes from the vertical symmetry axis of the network, and the higher the order of the branched system, the larger is the amount of a stream that is channeled to the outer branches of the network. This biased transport of substance toward the outer channels determines the shape of the concentration profiles generated at the outlets of the network.

Periodic Gradients. There are two ways to generate periodic gradients. One way is to use a microfluidic network with an appropriately large number of inlets. It is more convenient, however, to generate the concentration profile by combining multiple pyramidal networks in a parallel way. By following this latter approach, a broad range of concentration profiles can be generated using a small number of inlets. Figure 3 shows three examples of periodic gradients we realized by combining, in parallel, three networks each having two inlets. Since we can independently generate three different linear concentration profiles (each in one network), a variety of sawtooth gradients can be established when the individual profiles are brought together in the broad channel. Figure 3b demonstrates the generation of a sawtooth gradient, where the amplitude of the peak and the slope of the individual linear gradient decrease from the left to the right. Figure 3c shows a similar kind of gradient, where the difference between maximum and minimum concentration in all periods is

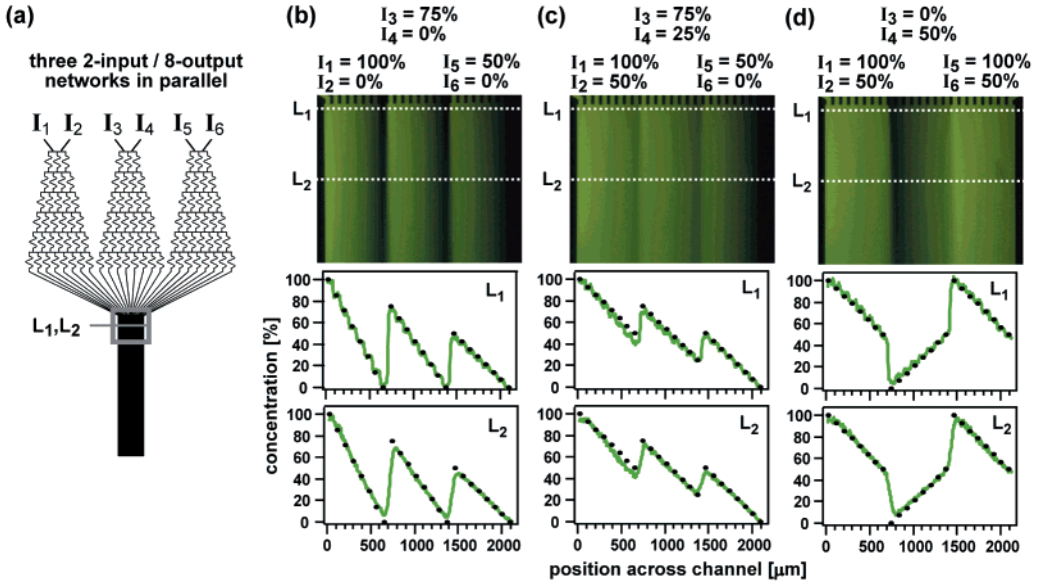

Figure 3. Fluorescence micrographs of three different sawtooth gradients of fluorescein in solution. The schematics (a) on the left of the micrographs show the design of the pyramidal network we used. The fluorescein concentration of the solutions we introduced into the inlets of the microfluidic device are shown above the individual gradients (b−d). The plots below the micrographs show the corresponding fluorescence intensity profile across the broad channel (2160 μm wide) at the beginning of the channel (L_1, white dotted line) and 800 μm downstream from the junction (L_2, white dotted line). The numerically calculated concentration profiles of fluorescein in the channel are shown as black round dots. The flow rate in the broad channel is 0.8 mm/s.

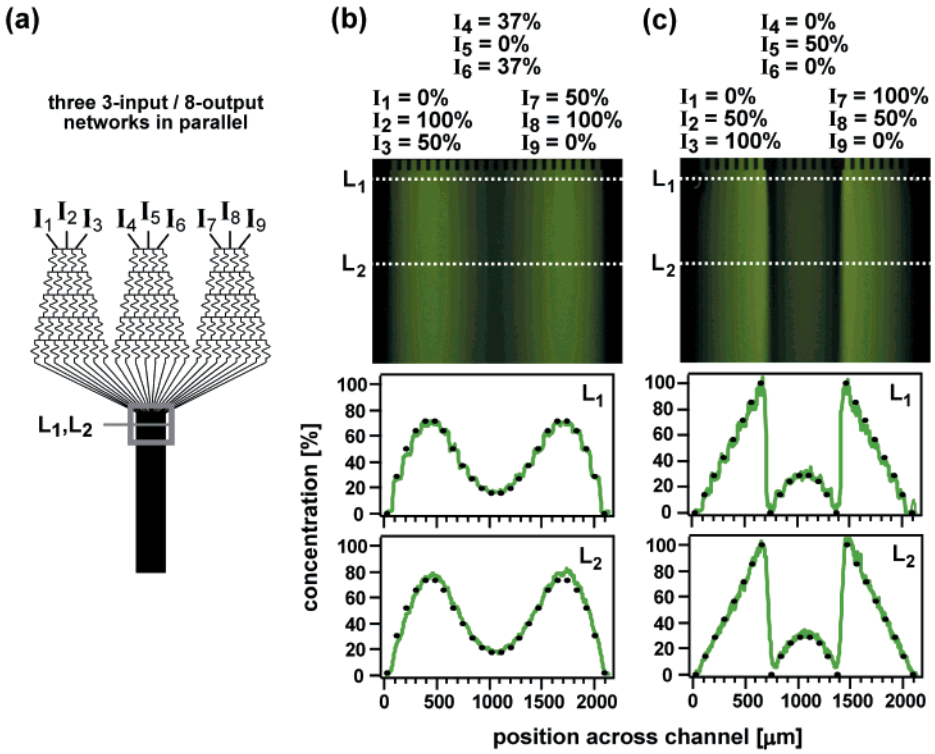

Figure 4. Fluorescence micrographs of two different periodic gradients consisting of parabolic parts (b) and a mixture of parabolic and linear parts (c). The schematic (a) on the left of the micrographs show the design of the pyramidal networks. The fluorescein concentration of the solutions we introduced into the network is given above the micrographs. The plots below the micrographs show the corresponding fluorescence intensity profile across the broad channel (2160 μm wide) at the beginning of the channel (L_1, white dotted line) and 800 μm downstream from the junction (L_2, white dotted line). The calculated concentrations of fluorescein in the channel are shown as round dots. The flow rate in the broad channel is 1.2 mm/s.

kept constant but the absolute maximum and minimum concentration decreases from the left to the right. Figure 3d shows a sawtooth gradient assembled from linear gradients with negative and positive slopes. In all three examples (Figure 3), we determined the concentration profile directly after the junction (L_1) and 800 μm downstream (L_2). At L_1 the initial small steps in the concentration profile can be seen in fluorescence; the observation of discernible steps indicates that diffusive mixing across the

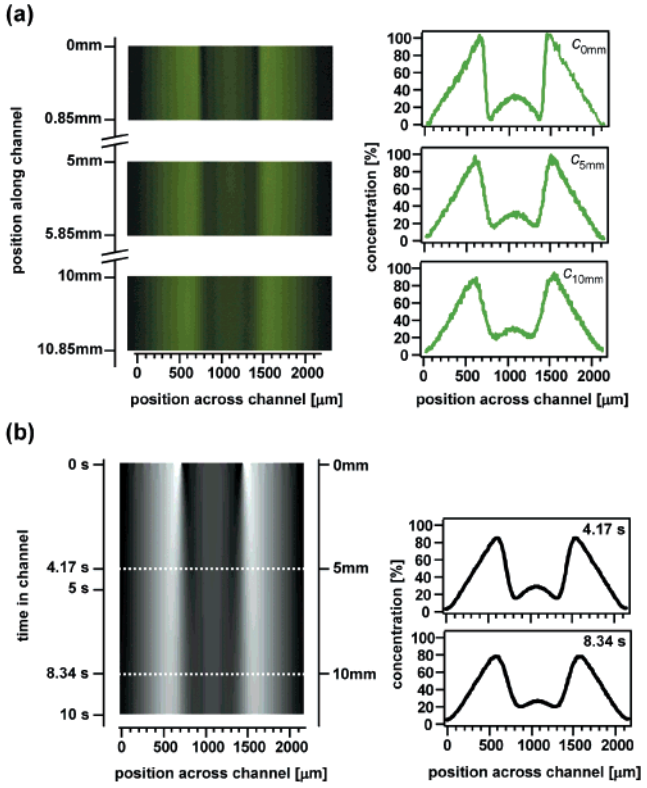

Figure 5. (a) Dissipation of a gradient in the main channel as a consequence of lateral diffusion. Distances refer to the point in the channel at which the gradients are formed by combining the individual streams. The corresponding concentration profiles are depicted in the graphs on the right side. (b) Numerical calculation of the concentration profile in the channel by using the diffusion equation in one dimension. The intensity plot (simulated picture) on the left side shows the distribution of the fluorescein in the channel; distances and the equivalent times are given on the right and left sides, respectively. The graphs on the right side show the intensity profile at 5 (4.17 s) and 10 mm (8.34 s) downstream the channel. The flow rate in the broad channel is 1.2 mm/s.

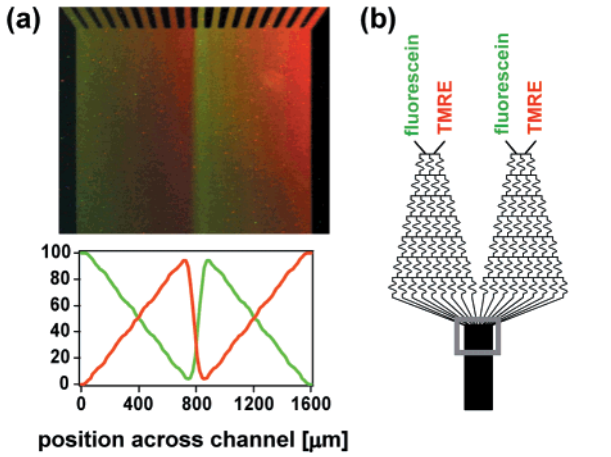

Figure 6. (a) Fluorescence micrographs of a periodic overlapping sawtooth gradient of fluorescein and TMRE in ethanol. The plot below the micrograph shows the numerically calculated fluorescence intensity profile across the broad channel (1620 μm wide) for the individual dyes at 1 mm (1 s) downstream the channel (using $D = 5.0 \times 10^{-6}$ cm^2/s for both dyes). The colored specs in the fluorescence micrographs are an artifact produced by the CCD camera when operating in integration mode. (b) A schematic of the microfluidic network we used.

boundary of the individual streams was not complete. In contrast, at L_2 (800 μm downstream; flow rate 800 μm/s; 1 s after combination at the junction), the steps have disappeared due to diffusion and the gradient is smooth. Numerical calculations of the diffusive mixing (using $D = 5.0 \times 10^{-6}$ cm^2/s) confirm that the small steps of the profiles, which have a periodicity of 90 μm, decay after ~1 s.

Increasing the number of inlets from two to three at the individual networks extends the accessible range of profiles, since composite gradients with parabolic parts can be generated. Figure 4b shows a symmetric gradient consisting of three parabolic parts. Since linear gradients are accessible with networks having three inlets, mixed gradients consisting of linear as well as parabolic parts can be generated (Figure 4c). As in Figure 3, we determined the concentration profiles at two positions in the channel. The observed and calculated profiles are in good agreement.

Although elastomeric PDMS structures with such low aspect ratios are prone to sag, we had no experimental indication that the fluid streams and therefore the shape of the concentration profile were distorted due to this effect.

Blurring of the Concentration Profile. Figure 5a shows the blurring of the concentration profile due to diffusion at three different positions downstream in the channel. The diffusional decay is described by the diffusion equation in one dimension, $\partial c/\partial t = D(\partial^2 c/\partial x^2)$, where D is the diffusion coefficient, c the concentration of the substance, and x the coordinate perpendicular to the direction of the fluid flow. Using a diffusion coefficient of 5.0×10^{-6} cm^2/s for fluorescein in water and taking into account the flow rate of the fluid through the broad channel, we calculated numerically the concentration profile established over the entire channel (Figure 5b) (The numerical calculation of the diffusive initial value problem was done using a forward time centered space (FTCS) differencing scheme[20]). The theoretical calculations are in good agreement with the experimentally observed concentration profiles (Figure 5b). The rate of blurring of individual concentration profiles depends on the shape of the gradients and has to be determined for every profile separately using the diffusion equation. In general, the largest changes occur in the area where the curvature ($\partial^2 c/\partial x^2$) of the gradients is the largest. In our example, these occur at the junction between the linear and the parabolic parts of the profile (at 720 and 1440 μm of the profile).

Superposition of Gradients. Another advantage of this approach is the potential to establish several gradients of different shapes simultaneously. Figure 6 shows an example of two sawtooth gradients of green (fluorescein) and red (tetramethyrhodamine ethyl ester, TMRE) fluorescent dyes in ethanol. They are generated by feeding the inlets of the system with mixtures containing different substances. Using this approach, complex and periodic gradients of different substances can be easily superimposed. Overlapping gradients provide a platform for comparing and quantifying the role of competing gradients in chemotaxis.

(20) Press: W. H.; Teukolsky, S. A.; Vetterling, W. T.; Flannery, B. P. *Numerical recipes in C*, 2nd ed.; Cambridge University Press: New York, 1999.

CONCLUSION

In this approach to the generation of gradients, we used two features of diffusion: (i) Step profiles with a step width of ~90-μm decay quickly by diffusion in water; rapid equilibration on the micrometer scale makes possible the generation of smooth gradients by approximating them with step gradients with appropriate and easily achievable step size and allows differences to smooth the steps over times of seconds. (ii) Gradients being extended over several hundreds of micrometers are stable over long periods of time, since diffusion is a slow process on the millimeter scale. Therefore, gradients across the broad channel (900−2100-μm width) are maintained over several tens of seconds, which is longer than the time the stream requires to travel downstream to the outlet. As a consequence, gradients in concentration formed at the junction of the broad channel are maintained, although slightly blurred due to diffusion, in the channel.

In contrast to most alternative techniques, in which the shape of the gradients evolves spatially with time, gradients generated using the microfluidic approach are spatially and temporally stable. Experiments where the shape of the gradient must be carefully defined and must be constant over long periods of times will benefit from this stability.

ACKNOWLEDGMENT

This work was supported by DARPA and NSF (ECS-9729405). S.K.W.D. thanks the DFG (Deutsche Forschungsgemeinschaft) for a research fellowship.

Received for review September 21, 2000. Accepted December 21, 2000.

AC001132D